Published online 12 October 2020 *Nucleic Acids Research, 2020, Vol. 48, No. 19* **10691–10701**
doi: 10.1093/nar/gkaa835

Cross-Inhibitor: a time-sensitive molecular circuit based on DNA strand displacement

Chanjuan Liu[1,†], Yuan Liu[1,†], Enqiang Zhu[2,*], Qiang Zhang[1,*], Xiaopeng Wei[1,*] and Bin Wang[3]

[1]School of Computer Science and Technology, Dalian University of Technology, Dalian 116024, China, [2]Institute of Computing Science and Technology, Guangzhou University, Guangzhou 510006, China and [3]Key Laboratory of Advanced Design and Intelligent Computing, Dalian University, Dalian 116622, China

Received September 22, 2019; Revised September 14, 2020; Editorial Decision September 16, 2020; Accepted September 18, 2020

ABSTRACT

Designing biochemical systems that can be effectively used in diverse fields, including diagnostics, molecular computing and nanomachines, has long been recognized as an important goal of molecular programming and DNA nanotechnology. A key issue in the development of such practical devices on the nanoscale lies in the development of biochemical components with information-processing capacity. In this article, we propose a molecular device that utilizes DNA strand displacement networks and allows interactive inhibition between two input signals; thus, it is termed a cross-inhibitor. More specifically, the device supplies each input signal with a processor such that the processing of one input signal will interdict the signal of the other. Biochemical experiments are conducted to analyze the interdiction performance with regard to effectiveness, stability and controllability. To illustrate its feasibility, a biochemical framework grounded in this mechanism is presented to determine the winner of a tic-tac-toe game. Our results highlight the potential for DNA strand displacement cascades to act as signal controllers and event triggers to endow molecular systems with the capability of controlling and detecting events and signals.

INTRODUCTION

DNA nanotechnology focuses on the design and manufacture of artificial nucleic acid structures and exploits DNA as the engineering material for technological uses (1,2), and it has promising applications in DNA computing (3,4), molecular self-assembly (5–7), disease diagnosis (8,9), etc. Due to the highly reliable specificity and predictability of DNA base-pairing, DNA molecules have received increased attention in recent years regarding the development of a variety of satisfactory devices, such as biosensors (10), probes (11,12), timers (13), computers (14–16), logic gates (17,18), nanolevers (19) and nanomachines (20–22).

Initially focused on the self-assembly of static structures (23), DNA nanotechnology for engineering systems with dynamic properties is attracting considerable attention; however, this attention is focused on forming nucleic acid systems with designed dynamic functionalities related to their overall structures; thus, these systems are known as 'dynamic DNA nanotechnology'. A DNA strand displacement reaction is a molecular dynamic process in which a single strand undergoes a structural reaction with part of a complementary double strand that replaces and releases the constrained single strand in the original double strand, thereby generating a new double stranded structure (24). Such strand displacement can be triggered when short, complementary single-strand domains (referred to as *toeholds*) are recognized, and it then progresses via branch migration that resembles a random walk (24–27). Generally, DNA strand displacement circuits are enzyme-free. Compared with enzyme-involved circuits, enzyme-free circuits seem more flexible since enzymes usually work under specific conditions, which may make the underlying methods more complicated and increase the cost of biochemical experiments (28).

The DNA strand displacement technique has been widely used to create a variety of synthetic molecular systems in recent years, such as adaptive networks (29), logical circuits (30,31), catalytic amplification (32,33), triggered structure assembly (24,34), autonomous molecular motors (35–37) and cargo-sorting DNA robots (38). Qian and Winfree (39) proposed a logic gate based on DNA strand displacement networks called a *seesaw gate*, which can be used as a simple building block for large-scale circuits

*To whom correspondence should be addressed. Tel: +86 2039366413; Fax: +86 2039366413; Email: zhuenqiang@gzhu.edu.cn
Correspondence may also be addressed to Qiang Zhang. Tel: +86 41187403733; Fax: +86 41187403733; Email: qzhangdl@163.com
Correspondence may also be addressed to Xiaopeng Wei. Tel: +86 41187403733; Fax: +86 41187403733; Email: xpweidl@163.com
†The authors wish it to be known that, in their opinion, the first two authors should be regarded as Joint First Authors.

and neural networks (15,40). Zhang *et al.* (34) realized the programmability of self-assembly kinetic control and showed that DNA strand displacement circuits and DNA tile self-assembly can be integrated systematically. Zhou *et al.* (41) constructed an active plasmonic system where a plasmonic nanorod functions as a walker to execute missions with some controllable, bidirectional, and progressive movements that are commanded through DNA strand displacement. More detailed information on this topic can be obtained in the literature (42–44).

Given the significance of developing biochemical components with information-processing capacity for the production of practical molecular systems, we are interested in the design of DNA strand displacement circuits for the processing and control of signals and events within biochemical systems at the nanoscale. Rather than only addressing DNA strand concentrations, the circuit here is intended to respond to the timing of consecutive events.

More specifically, we propose a molecular device that utilizes DNA strand displacement networks, and it is called a *cross-inhibitor*. Consisting of two bifunctional processors that can receive upstream signals and produce inhibitory signals, this device promotes interactive inhibition between two input signals. Technically, the processors are expected to achieve 'two functions': the first is to react with a corresponding upstream signal and release an inhibitory signal; and the second is to inhibit the other processor by this inhibitory signal. To receive different signals and carry out branch migrations in both directions, each of the two processors in our design contains a toehold with one domain each on its left and right sides.

The work most related to ours is (45), which proposed a cross-catalyst circuit such that two signal receivers can take each other's output as their own input. The goal of this circuit is to implement a catalytic reaction. The cross-inhibitor, however, is expected to be used in molecular circuits in which the timing of events is critical, such as the circuit for detecting the temporal order in which two signals have emerged. Based on the mutual inhibitory effect, the cross-inhibitor can also be applied to the fields of information security, automatic control, etc. to build some devices for molecular encryption (46), circuit control (47), etc. Moreover, by applying a mismatch strategy, the cross-inhibitor can be transformed to asymmetrical-inhibitor to meet some special requirements, e.g. to participate in the construction of analog circuits.

As an illustration of the effectiveness of the cross-inhibitor, a biochemical framework grounded in this mechanism is presented in which the inhibitor acts as a 'referee' and judges the winner of a tic-tac-toe game. In (48), tic-tac-toe was encoded by a molecular automaton to compete against a human opponent. However, it utilized a deoxyribozyme-based logical strategy, whereas the cross-inhibitor is enzyme-free with a simpler design. In addition, the cross-inhibitor is not dedicated for tic-tac-toe, which is only provided as a test-case.

The remainder of this paper is organized as follows. We first present the methods and principles used in designing our cross-inhibitor. Then, the feasibility of this mechanism is demonstrated by an analysis of the results obtained with different orders of the two input signals. The performance of the cross-inhibitor in terms of the time response is investigated via varying the time intervals between adding the two input signals. Further experiments show that the cross-inhibitor can be regulated dynamically as expected under appropriate signal stimulations. In addition, the asymmetric inhibition in the sense that one processor is more inhibited than the other is realized by base-mismatch. Finally, the game of tic-tac-toe is taken as a test-case of the proposed cross-inhibitor. Since the design of this framework is modular, it provides an effective interface for establishing biochemical circuits and detecting molecular sensors. Our results also highlight the potential for DNA strand displacement cascades to act as signal controllers and event triggers, among other functions, to endow molecular systems with the capability of controlling and detecting events and signals.

MATERIALS AND METHODS

Materials and reagents

All DNA samples with sequences were synthesized by Takara Biotechnology Co., Ltd. (Dalian, China). Unmodified DNA strands were gel purified via polyacrylamide gel electrophoresis (PAGE), and modified DNA strands were purified via high-performance liquid chromatography (HPLC). All oligonucleotides were dissolved in 1× Tris-acetate–EDTA-Mg^{2+} (1×TAE/Mg^{2+}) buffer (40 mM Tris, 20 mM acetic acid, 1 mM EDTA2Na and pH balanced to 8.0 (purchased as 50× stock from Solarbio Science & Technology Co., Ltd.), to which 12.5 mM $Mg(OAc_2)$ was added) and stored at 4°C. the DNA sample concentration was measured by a NanoDrop 2000 spectrophotometer (Thermo Fisher Scientific Inc., USA), and the absorption wavelength was set to 260 nm. All the involved reagents were of analytical grade without further purification. All solutions were prepared using deionized water. Note that PAGE purifications were not applied in our experiments.

Assembly procedure

All DNA complexes (listed in Supplementary Table S1) were assembled by mixing the corresponding single strands with equal molar concentrations (4 μM) in 50 μl 1× TAE/Mg^{2+} buffer. All samples were annealed in a polymerase chain reaction (PCR) thermal cycler. The temperature was set at 95°C for 5 min initially, decreased to 65°C at a rate of −0.8°C every minute, and finally decreased to 20° at a rate of −0.5° every minute.

DNA sequence design

The sequences of all strands in the experiment as listed in Supplementary Table S2 are designed in the following process: the original sequences were obtained by using Nupack, which were then modified by hand. These modified sequences were further inspected by Nupack to avoid unexpected hybridization structures (Supplementary Tables S3 and S4) and reduce crosstalk between unrelated domains. The domain sequences used in the designed device are given in Figure 1C.

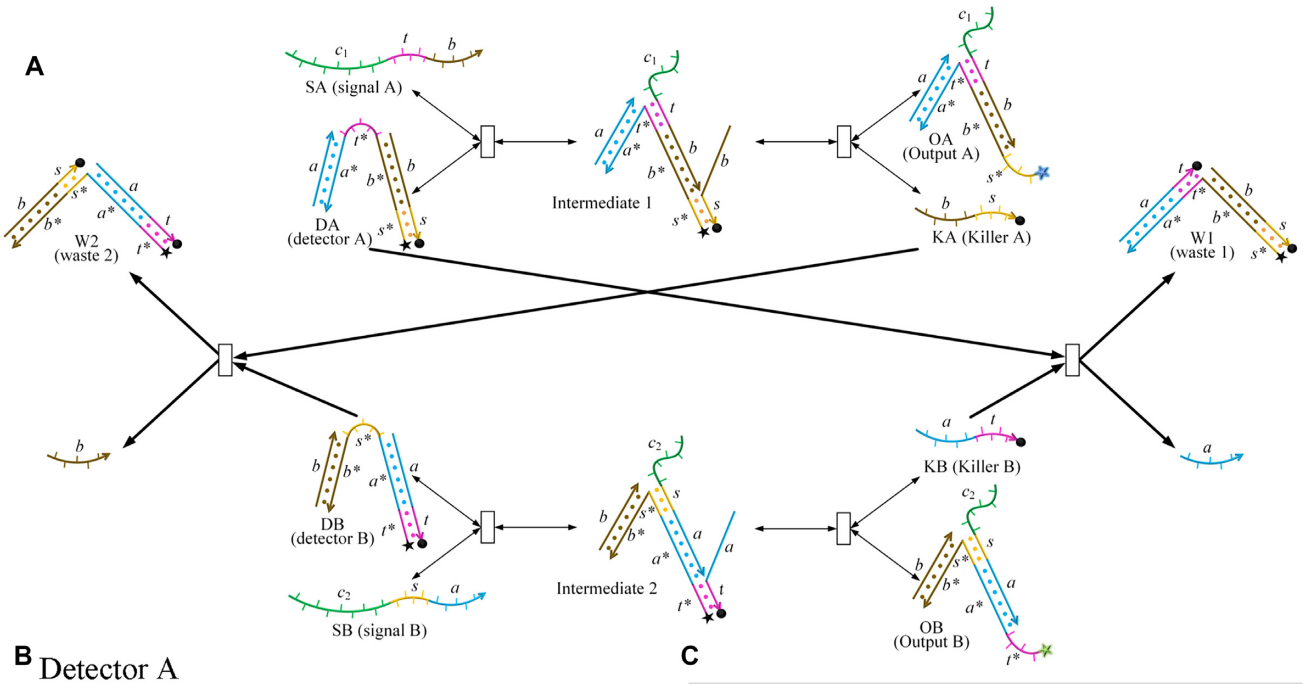

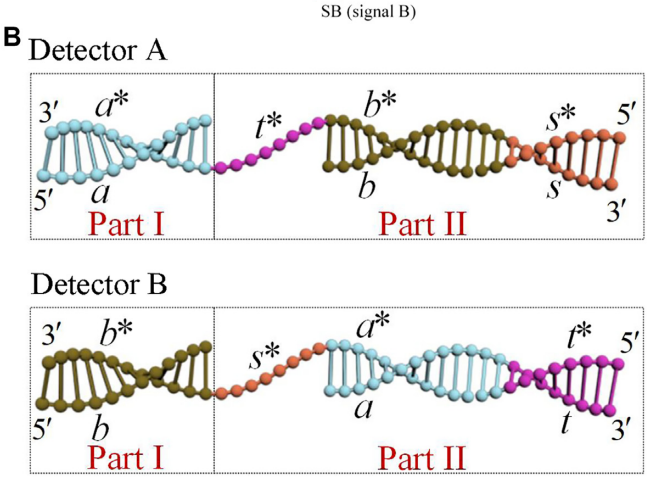

C

Domain	Sequence (5′ → 3′)	Length (nt)
a	CATCCACTAGCACACACTGAGAC	23
b	GTAACGTTGGACTCTCGTCACTG	23
t	ATGCAC	6
s	TCGTAC	6
c_1	CAGTATCT	8
c_2	TACATTCA	8

Figure 1. Principle of the cross-inhibitor. (**A**) Schematic illustration of the cross-inhibitor principles. Here, due to the strand displacement of SA (resp. SB) by DA (resp. DB), the output KA (resp. KB) is able to consume a number of DB (resp. DA), which results in cross-inhibition. (**B**) Illustration of the structures of detectors. Both DA and DB are composed of abstract domains *a*, *b*, *t* and *s* and can be partitioned into two parts: I and II. (**C**) Domain sequences of the cross-inhibitor.

Displacement reaction to trigger cross-inhibition

The DNA strand displacement reaction was triggered in 1× TAE/Mg^{2+} buffer at 25°C. The input signals represented by DNA strands were added to a solution containing 'detectors' and logic gates.

Nondenaturing polyacrylamide gel electrophoresis (PAGE)

The DNA solutions mixed with 50% glycerine solution were analyzed in a 12% native polyacrylamide gel in 1× TAE/Mg^{2+} buffer after running for 120 min at a constant voltage of 80 V. Gels were stained with Stains-all, which was purchased from Sangon Biotech Co., Ltd. (Shanghai, China), and scanned with a scanner (CanoScan LiDE 120).

Fluorescence kinetics

All spectrofluorometric measurements were performed at 25°C using a real-time PCR system (Agilent, G8830A) equipped with a 96-well fluorescence plate reader. All samples were incubated at 25°C in 1× TAE/Mg^{2+} buffer. The volume of each DNA sample was 25 μl.

Simulation

Simulation and dynamic analysis were implemented on Wolfram Mathematica 12.0 using CRNSimulator. CRNSimulator Mathematica Package (CRNSimulator.m) and its extensions (CRNSimulatorExtensions.m) were loaded before running the program. In the program, the unknown parameters in the chemical reaction model were estimated based on the experimental data.

PRINCIPLE OF THE CROSS-INHIBITOR

The principle of the cross-inhibitor is presented in Figure 1A. This cross-inhibition mechanism can be expressed via the following reactions:

$$\mathrm{SA} + \mathrm{DA} \underset{k_2}{\overset{k_1}{\rightleftharpoons}} \mathrm{KA} + \mathrm{OA} \tag{1}$$

$$\mathrm{KA} + \mathrm{DB} \xrightarrow{k_3} W1(\text{waste 1}) + b \tag{2}$$

$$\mathrm{SB} + \mathrm{DB} \underset{k_5}{\overset{k_4}{\rightleftharpoons}} \mathrm{KB} + \mathrm{OB} \tag{3}$$

$$\mathrm{KB} + \mathrm{DA} \xrightarrow{k_6} W2(\text{waste 2}) + a \tag{4}$$

The critical components in the circuit are two three-stranded substrate complexes, which are called *detectors* and denoted as detector A (DA) and detector B (DB). The structures of these two detectors are key in achieving the effect of 'cross-inhibition'. Note that DA and DB are composed of the same set of abstract domains, viz., a, b, t and s, but differ in the order of these domains. The domains a and b are referred to as *specificity domains*, while t and s are referred to as *toehold domains* (45). As further illustrated in Figure 1B, both detectors can be partitioned into two parts, namely, I and II, where part II is designed based on the principles of the *seesaw gate* (39). A seesaw gate is a DNA molecular module that leverages a reversible strand displacement reaction based on the principle of toehold exchange, which is reliable in the composition of large-scale biochemical integrated circuits since the structural similarity between its input and output beneficially allows the output of one seesaw gate to be the input for another seesaw gate. In addition, the domain a (in part I) of DA is exactly that (in part II) of DB while the domain b (in part I) of DB is the same as that (in part II) of DA.

The structures of detectors make the cross-inhibition possible. For DA, when the input SA is added, the toehold t of SA will bind to the domain t^* of DA, and then branch migration will move gradually to toehold s, which will release a single-strand KA together with a desired beacon-labeled output OA for real-time monitoring, where KA carries a quencher at its 3′ end and OA carries a fluorophore at its 5′ end. Once KA is produced, it can consume detector B since the toehold s of KA will recognize the s^* of DB and initialize the branch migration to b. This process generates the stable double helix Waste 2.

Suppose that we first add the input SA into the biochemical reaction circuit. A sequence of reactions will be activated, after which a portion of DB will be consumed. Naturally, this process will lead to the inhibition of the reaction between SB and DB when SB is added later. The process of inhibiting SA with KB can be obtained by symmetry. Observe that when the two directions of inhibition occur simultaneously, a cross will be formed in the reaction network and this explains the reason why this motif is called a 'cross-inhibitor'.

RESULTS AND DISCUSSION

Feasibility of cross-inhibition

The performance of the cross-inhibitor circuit was investigated via a PAGE gel as shown in Figure 2A. Lanes 5, 6, 7 and 8 are reference substances, in which we added only DA and DB, waste 1 and waste 2, OA and SA, and OB and SB, respectively. Both lanes 1 and 2 contain DA and DB; the difference is that SA is added to lane 1 while SB is added to lane 2. Compared with lanes 1 and 2, in lanes 3 and 4, SB and SA are added after 40 min, respectively. Compared with lane 7, in lane 1, SA can react with substrates (DA and DB) to form OA when SB is not present. Similarly, compared with lane 8, in lane 2, SB can react with substrates (DA and DB) to form OB when SA is not added. Although lane 3 and lane 4 share the same inputs, due to the order of the inputs, more OA is produced in lane 3 while more OB is produced in lane 4, which reflects the cross-inhibition.

Figure 2B presents the results of the fluorescence experiment and side-by-side comparisons with the simulation data. DA and DB are added as substrates in advance. In the left panel of Figure 2B, the OA-data and OB-data curves show the intensity of OA and OB, respectively, when SA is added first and SB is added after 30 min. The curves show that the OA-data fluorescence increases rapidly once SA is added and is then slightly prevented after SB is added. The final level of OB-data fluorescence is lower than that of OA-data fluorescence because a portion of DB has already been consumed by KA. Note that not all DB is consumed by KA since the reaction rate of KA with DB is lower than that of SA with DA. Meanwhile, the time period for KA reacting with DB is limited (viz. 30 min). The dotted lines show the simulation results using experimentally measured rate constants, with $k_1 = 7.5 \times 10^4$, $k_2 = 1.7 \times 10^5$, $k_3 = 2.6 \times 10^4$. Note that the rates $k_1, \ldots, k_6$ are the same for other figures with simulation results in the paper, since the same sequences and experimental conditions are used. Due to the approximate symmetry of the reactions for DA and DB, we assume that $k_1 = k_4$, $k_2 = k_5$, $k_3 = k_6$. In the right panel of Figure 2B, the OA-data and OB-data curves represent the corresponding results when SB is added 30 min earlier than SA. The similarity of the results in these two cases provides strong support for the feasibility of our circuit. The agreement of the experimental data and simulation results suggests that simulations can be a useful guide for predicting the cross-inhibitor performance.

Further fluorescence experiments are conducted to determine the degree to which one signal will be inhibited. Particularly, we consider the influence of two factors, viz., the concentration ratio of the input signals to the detectors and the absolute concentrations of the detectors. We define the *inhibition degree* of DB by DA at time t (denoted by $id_t(B)$) as the ratio of concentration of OA to that of OB at t, i.e.,

$$id_t(B) = \frac{[OA]_t}{[OB]_t}.$$

Correspondingly, the inhibition degree of DA by DB at time t (denoted by $id_t(A)$) is the concentration ratio of OB

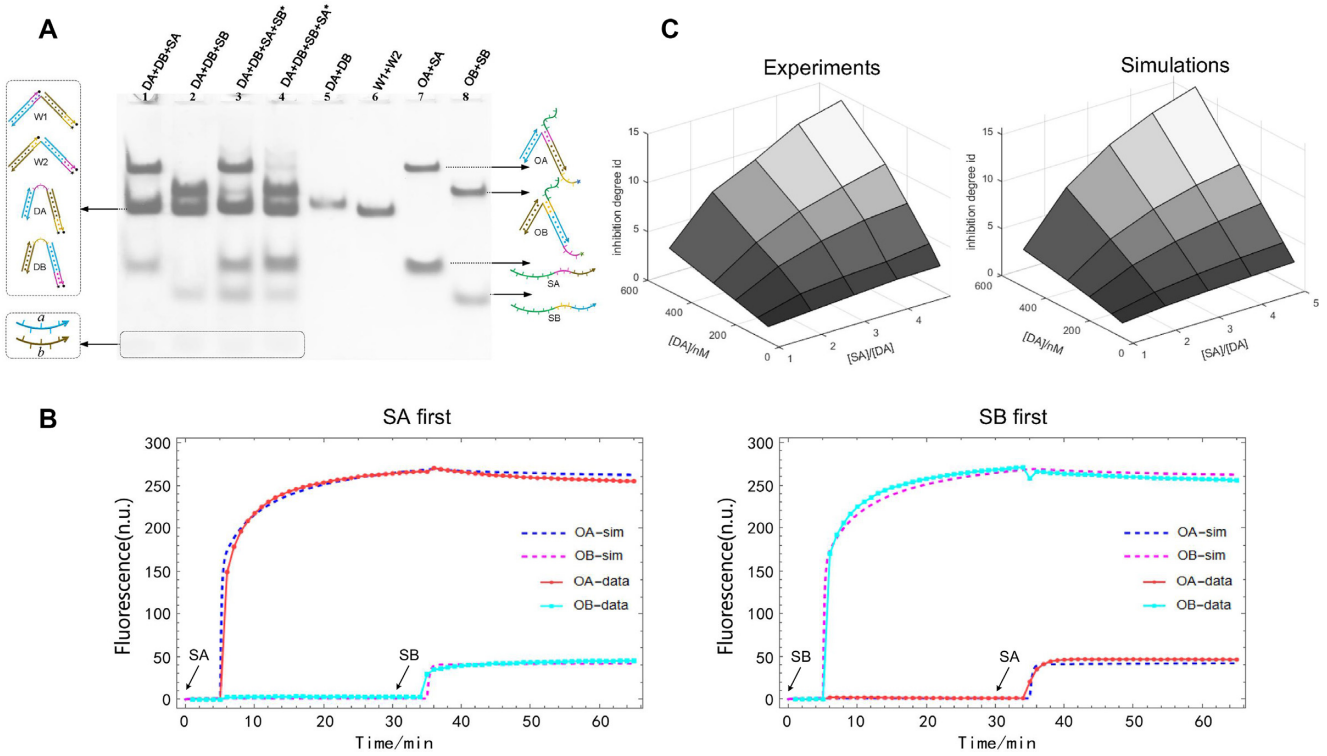

Figure 2. Feasibility of cross-inhibition. (**A**) Polyacrylamide gel electrophoresis (PAGE) illustration of cross-inhibition performance: the symbol '+' denotes the addition of the corresponding strand; the superscript '*' denotes that the corresponding strands were added after 40 min. Here, [DA] = [DB] = 300 nM, and [SA] = [SB] = 600 nM. See the supplementary materials (table S2) for sequences of these strands. (**B**) Kinetic characterization. Here, [DA] = [DB] = 300 nM, and [SA] = [SB] = 600 nM. DA and DB are added as substrates in advance. The X-axis denotes the quantitative real-time PCR at a frequency of 1 data point per minute and temperature of 25°C. The Y-axis denotes the relative intensity of each fluorescence. The measured fluorescence was normalized so that 1 normalized unit (n.u.) of fluorescence corresponds to the fluorescence signal generated by 1 nM DA. For the left figure, SA is added first and SB is added after 30 min; while for the right figure, SB is added first and SA is added after 30 min. (**C**) Experimental and simulations results on the tendency of inhibition degree $id_{120}(B)$ against the concentration ratio of the input signals to the detectors and the absolute concentration of the detectors. Here, the points with [DA] = {50, 100, 200, 300, 500 nM} and [SA]/[DA] = {1, 2, 3, 4, 5} are sampled, where for each point the equilibrium value of [OA] and [OB] are read at 120 min. We set [DA] = [DB] and [SA] = [SB]. The X-axis denotes the concentration of DA ([DA]), the Y-axis denotes the ratio of [SA] to [DA], and the Z-axis represents the inhibition degree. More details can be found in Supplementary Figures S1 and S2.

to OA at t, i.e.,

$$id_t(A) = \frac{[OB]_t}{[OA]_t}.$$

Based on the symmetry of the cross-inhibition mechanism, we check only the case when SA is added earlier than SB. Note that [SA] = [SB] and [DA] = [DB]. Figure 2C shows that there is an upward trend in the inhibition degree $id_{120}(B)$ with an increase in either of the two factors. The inhibition degree increases linearly with the increase of [DA], while the growth of the inhibition degree would flatten out with the increase of [SA]/[DA]. These dynamics may provide guidance for adjusting the parameters to attain the desired inhibition degree during the practical use of the cross-inhibition mechanism.

Time response characteristics

In previous experiments, one of the two input signals was added before the other, indicating that our circuit was time-related. Now, we analyze the characteristics of this circuit in terms of the time response via a series of experiments, with the results shown in Figure 3. We set the substrates DA and DB as [DA] = [DB] = 300 nM. SA with [SA] = 600 nM is first added, and there is a time interval before adding SB at the same concentration (600 nM).

Figure 3A shows the results of a fluorescence experiment together with the simulation data, where distinct time spans (namely, 5, 10, 20, 30 and 40 min) are selected. A longer interval corresponds to a lower intensity of OB because more KA is generated over time and thus more DB will be consumed.

Figure 3B shows the results of PAGE. Lanes 7–9 are the reference substances with wastes, OA, and OB, respectively. From lanes 1–5, the color depths of the bands corresponding to OB become weaker as the interval increases.

To quantify the influence of the time interval between adding the two input signals in the above fluorescence experiment, a chart shown in Figure 3C is drawn by polyfit in MATLAB. The circles in blue are the data obtained via bioexperiments, with the X-axis representing time intervals (viz., 5, 10, 20, 30 and 40 min) and the Y-axis showing the corresponding inhibition degree. This chart indicates that the inhibition degree increases as the time interval (within the range of 5–40 min) becomes larger.

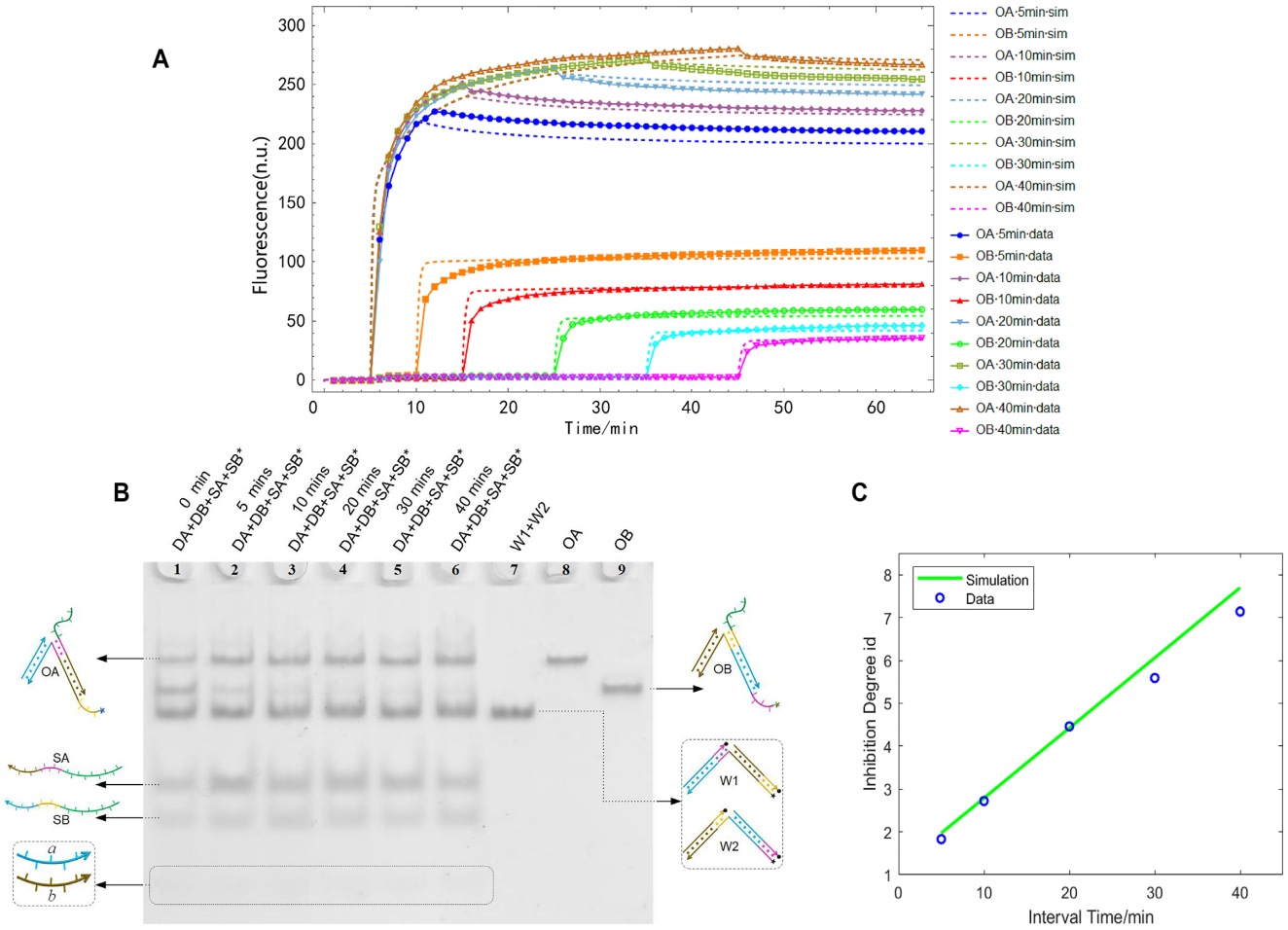

Figure 3. Time response characteristics. (**A**) Experimental and simulations results on fluorescence intensities for OB with different intervals (viz., 5, 10, 20, 30 and 40 min) before adding the input SB, where [DA] = [DB] = 300 nM and [SA] = [SB] = 600 nM. (**B**) The time response characteristics observed by PAGE (12% gel). DA and DB are added in advance as substrates. SA is added before SB at different intervals (viz., 5, 10, 20, 30 and 40 min), [DA] = [DB] = 300 nM, and [SA] = [SB] = 600 nM. To differentiate the bands in the PAGE gel, a 16-base poly-A tail was added to the 5′ end of SA and a 4-base poly-A tail was added to the 5′ end of SB. Note that Poly-A does not affect the strand displacement process; see Supplementary Figure S3. (**C**) Connection between inhibition degree and time interval measured by polyfit in MATLAB. SA is added before SB at different intervals (viz., 5, 10, 20, 30 and 40 min) as represented by the X-axis. The Y-axis shows the inhibition degree $id_{120}(B)$ for [DA] = [DB] = 300 nM and [SA] = [SB] = 600 nM.

Additional input schedules

For potential application in molecular systems of controlling signals and events, the circuit of the cross-inhibitor is expected to behave in a manageable manner. This section investigates its performance under multiple additional conditions.

As suggested by the reaction model of the cross-inhibitor and the experimental results in Figure 2C, the inhibition degree shows an upward trend when the concentration ratio of the inputs to the substrates are increased. Therefore, a natural issue is whether the cross-inhibition mechanism can perform as expected, viz., has a certain inhibition effect, when the concentration ratio is at a low level. In our experiment, The initial setting is the same as before, i.e. DA and DB are taken as substrates, with [DA] = [DB] = 300 nM. SA and SB are then added at different times and various concentrations. We mainly focus on the following three representative cases as shown in Figure 4. The function of the cross-inhibitor in these cases are as follows: detecting that two kinds of signals have the same intensity even if they occur at different times (in Figure 4A); inhibiting the later invading signal (in Figure 4B); and concealing the existing signal (in Figure 4C).

The results in Figure 4 suggest that the cross-inhibitor can be controlled dynamically, even when the concentration of the inputs is lower than that of the substrates. Thus, an effective response to various strong or weak input signals can be realized. The addition of one input may influence the different reactions, which enables real-time and sensitive regulation of DNA signals via the cross-inhibition mechanism. The consistency between the simulation and experimental data further supports that the cross-inhibitor functions are regulated as designed.

Asymmetric inhibition with base mismatch

While cross-inhibition allows for the bidirectional inhibition between two signals, it would be interesting to determine whether asymmetric inhibition is also possible. In some cases, it is useful when the inhibition towards one particular direction is preferred, e.g. inhibiting an unwanted

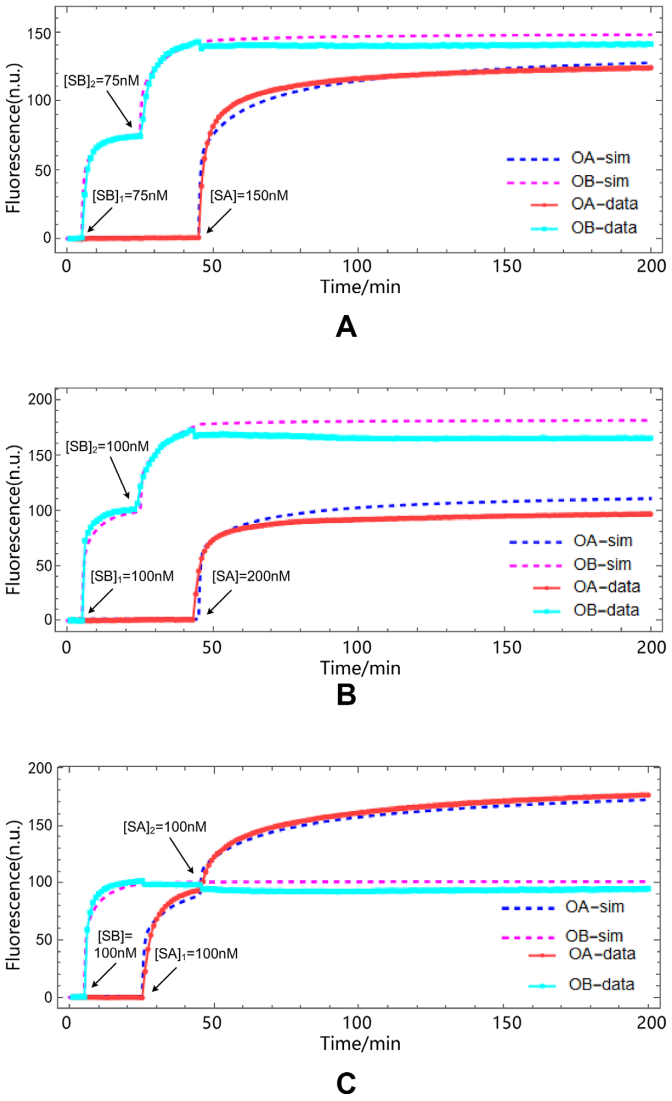

Figure 4. Dynamic controllability. In these three cases, DA and DB are taken as substrates with [DA] = [DB]= 300 nM. SA and SB are then added at different times with various concentrations. (**A**) Case 1: Obtaining the same intensity by different schemes. This experiment aims to demonstrate that with the regulation of the cross-inhibitor, two signals can finally be well matched, even if they are not added simultaneously. In our setting, the total amount of SA is the same as that of SB. The addition of SB is carried out in two separate steps, and SA is added all at once thereafter. That is, the first addition of SB is $[SB]_1 = 75$ nM, the second addition of SB is $[SB]_2 = 75$ nM, and then [SA] is added (150 nM). The cross-inhibitor ultimately equalizes the intensities of the output signals OA and OB. The dotted lines show the simulation results that reproduced the experimental data. (**B**) Case 2: Inhibition of the weaker signal that emerges later. In this situation, the cross-inhibitor helps inhibit the intrusion of an invasive signal. The addition of input signals is the same as in Case 1, but the concentrations are $[SB]_1 = 100$ nM, $[SB]_2 = 100$ nM and $[SA] = 200$ nM. Compared with Case 1, the SB signal is strong enough to consume a larger proportion of DA such that adding even an excessive amount of SA does not elicit a change. This behavior is confirmed by the simulations shown in dotted lines. (**C**) Case 3: Surpassing the early starters. Compared with case 2, this experiment shows the possibility of inhibiting a disturbance that appears earlier. A weaker signal SB is added first, with [SB] = 100 nM, and then a stronger signal SA is input in two steps with $[SA]_1 = [SA]_2 = 100$ nM. Since the substrate DB is largely consumed by KA, the output signal OB is distinctly weaker than that of OA despite the input of SB occurring at an earlier time. The dotted lines show the simulation results that reproduced the experimental data.

signal or participating in the construction of analog circuits. A single-base mismatch strategy was applied to regulate the process of strand displacement in (49). Inspired by this, we explore the approach to altering the inhibition pattern of our circuit.

Figure 5A shows five cases of base mismatch, where we change one or two base pairs next to the toehold *t* in specificity domain *a* of DA while leaving all other base pairs unchanged. The principle is that all the reactions can proceed normally except for the inhibition of DA by KB. While KA reacts with DB smoothly, the reaction of KB with DA is obstructed because of the base mismatch. Consequently, the effect of DA inhibition by KB will be much weaker than the effect of DB inhibition by KA, which leads to an 'asymmetric inhibitor'.

The asymmetric inhibition mechanism is tested by using a biochemical experiment for the five cases of base mismatch mentioned above. Figure 5B presents the results of two groups of fluorescence experiments on case 5. For the first group, SA is added 30 min before SB. In this case, DB is strongly inhibited by KA; therefore, there is a large gap between the final intensities of G1-OA and G1-OB. For the second group, SB is added 30 min before SA. However, for the sake of base mismatch, DA is inhibited weakly, which still allows G2-OA to achieve high growth after SA is added.

A comparative analysis of the effects of asymmetric inhibition based on the 5 different cases of base mismatch is shown in Figure 5C. Compared to the case without a base mismatch, the existence of a base mismatch in DA causes an increase in the inhibition of DB by DA and a decrease in the inhibition of DA by DB. This behavior further demonstrates the symmetric inhibition mechanism.

Application to tic-tac-toe

With the function of cross-inhibition, the cross-inhibitor can be used for observing and marking some biochemical processes. As an illustration of the feasibility of the cross-inhibitor, we design a biochemical framework grounded in this mechanism in which the cross-inhibitor can be used to monitor which player forms a line first and thus can serve as a 'referee' to judge the winner of a tic-tac-toe game.

Tic-tac-toe. Tic-tac-toe (also known as *noughts and crosses* or *Xs and Os*) is a game for two players, X and O, who take turns to mark the spaces in a 3 × 3 grid. The player who first succeeds in placing three consecutive marks in a (horizontal, vertical, or diagonal) row wins the game. Due to its simplicity, tic-tac-toe is often used as a pedagogical tool and an illustrative example in research on artificial intelligence (50,51). The spaces on the game board can be labeled with numbers 1 to 9 as shown in Figure 6A. Thus, each player has eight winning possibilities, i.e., placing three of their marks in a horizontal (123,456,789), vertical (147,258,369), or diagonal row (159,357).

For convenience, we define 9 game pieces for each player, which are denoted by x_i (or o_i), $i = 1, 2, \ldots, 9$; thus, player X (or player O) places a piece in space *i* (as shown in Figure 6A. Further, we define a winning set consisting of eight triples: $W = \{(1, 2, 3), (4, 5, 6), (7, 8, 9), (1, 4, 7), (2, 5, 8), (3, 6, 9), (1, 5, 9), (3, 5, 7)\}$. Notice that the triples here are

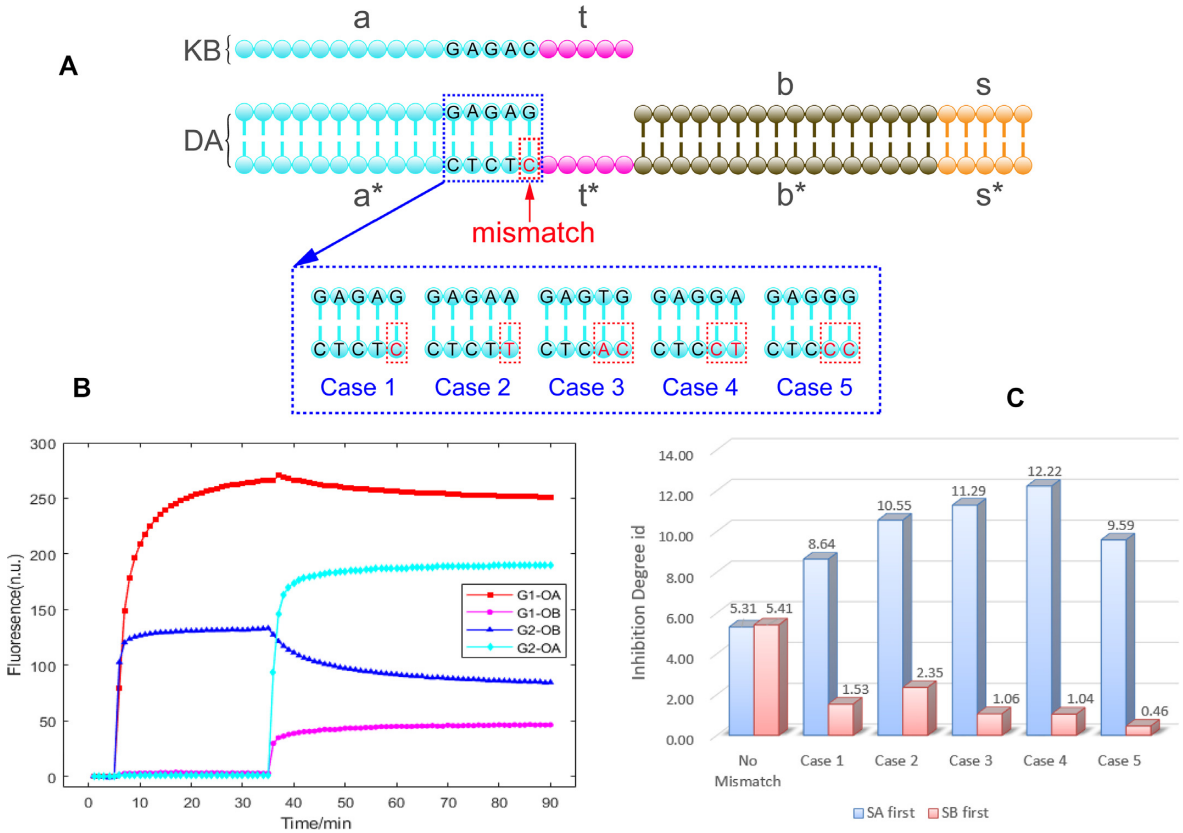

Figure 5. Asymmetric inhibition with base mismatch. (**A**) Five cases of base mismatch for the asymmetric inhibitor. In domains *a* and *a** of detector A, one or two bases are changed. The branch migration will be inhibited when KB comes to detector A and the toehold *t* binds to *t**. (**B**) Fluorescence intensity in the asymmetric inhibitor. G1-OA and G1-OB are the outputs of the first group, in which SA is added 30 min earlier than SB. In contrast, G2-OA and G2-OB are the outputs of the second group, in which SA is added 30 min after adding SB. In both groups, [DA] = [DB] = 300 nM and [SA] = [SB] = 600 nM. The other four cases containing different mismatch sequences are given in Supplementary Figure S4. (**C**) Comparison of inhibitor effects among the case without base mismatch and five cases with base mismatch. [DA] = [DB] = 300 nM, [SA] = [SB] = 600 nM. The X-axis lists the six cases (five cases of base mismatch together with the case without base mismatch). For each case, we compare the inhibition degree of DB by DA when SA is added earlier with the inhibition degree of DA by DB when SB is added earlier. That is, for each case, the first bar shows id_{120}(B) when SA is added 30 min earlier than SB, and the second bar shows id_{120}(A) when SB is added 30 min earlier than SA. Compared to the case without a base mismatch, the existence of a base mismatch in DA causes an increase in id_{120}(B) and a decrease in id_{120}(A).

unordered. If one player (e.g. X) places three pieces x_i, x_j, and x_l (in any order) to form a straight line first (that is, (i, j, l) $\in W$), then X wins. Correspondingly, if O places three pieces to form a straight line first, then O wins. Otherwise, the game ends in a draw. For the game shown in Figure 6A, player X wins.

Circuit design. In 2003, tic-tac-toe was encoded by a molecular automaton to compete against a human opponent based on a deoxyribozyme-based logical strategy (48). Here, we are interested in an enzyme-free circuit utilizing our cross-inhibitor, which can act as a referee to decide the winner of this game based on a strategy called *winner-take-all*, which was initially applied to a biochemical network in (52).

In our design, game pieces for the two players are placed sequentially into one tube to imitate the process of playing tic-tac-toe. A biochemical circuit for this game should have two main functions: detecting whether a (horizontal, vertical, or diagonal) row has been formed and determining the player that wins the game (i.e., who makes a line first).

This game circuit consists of two modules: three-input AND gates (53) and the cross-inhibitor proposed above. The function of the three-input AND gates is to recognize the existence of a line. As long as one line is formed by a player, this module will release a victory signal that can be received by the cross-inhibitor, which can then output a fluorescence signal to declare the winner.

More specifically, the three-input AND gates are of two types, with one for each player X and O. For each (i, j, l) $\in W$, the gate for X is denoted by X-ijl, which can receive (in any order) the three input strands corresponding to pieces x_i, x_j and x_l and can be activated if and only if all these three input signals are present. Figure 6B illustrates how X-456 is activated by the inputs x_4, x_5 and x_6, which is followed by the release of SA to trigger the cross-inhibitor; and the gate O-357 for O can be activated when the three inputs x_4, x_5 and x_6 are presented and then release SB to trigger the cross-inhibitor. Other gates work similarly.

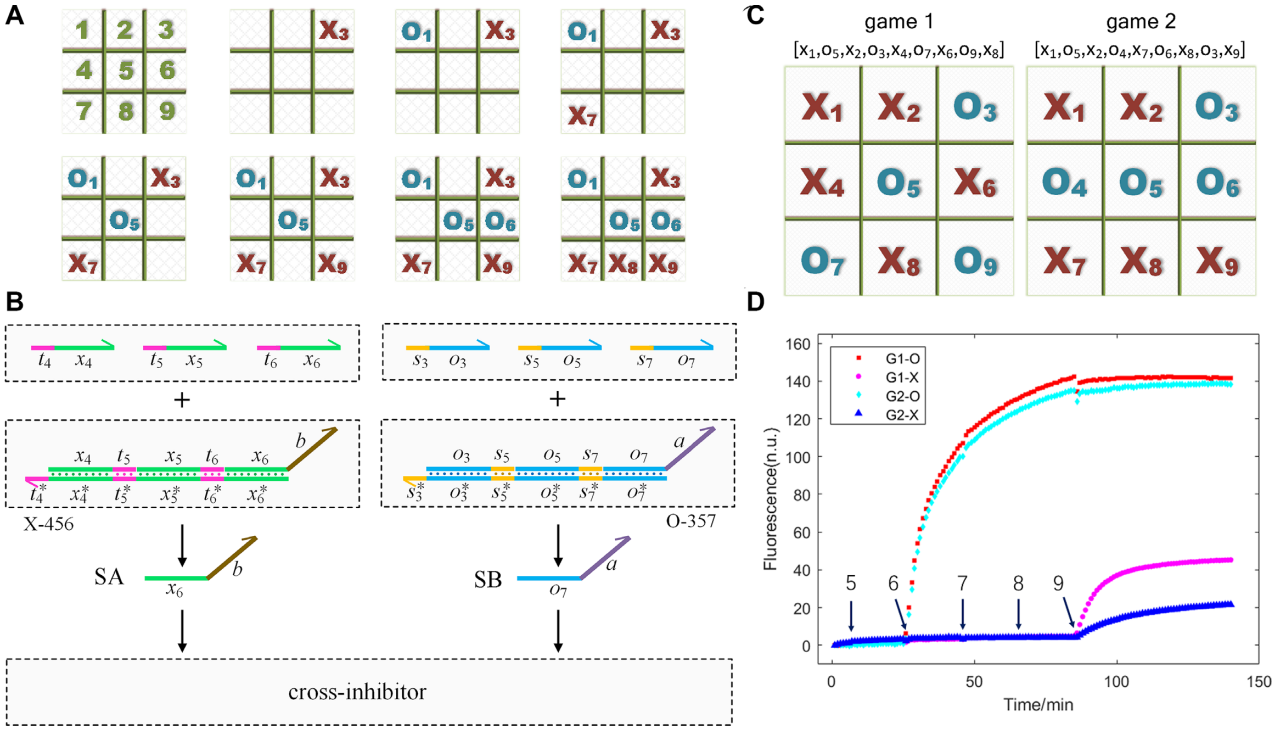

Figure 6. Application to tic-tac-toe. (**A**) The game of tic-tac-toe. (**B**) Schematic diagram of the three-input AND gates. The interaction process between the cross-inhibitor and the outputs of three-input AND gates is shown in Supplementary Figure S5. The 'capping-technique' is adopted to reduce the leakage; see Supplementary Figure S6. (**C**) Two examples of a tic-tac-toe game for testing the circuit. (a) Game 1: only player O produces a line. (b) Game 2: player O forms a line earlier than X. (**D**) Real-time monitoring of the fluorescence intensity for two tic-tac-toe games. Since no winner can be yielded in the first three steps, the monitoring of the results starts in the fifth step. Each number in the chart represents the corresponding step. For game (1), the fluorescence for O (i.e. G1-O) begins to increase in the sixth step while the fluorescence for X (i.e. G1-X) almost remains the same until the ninth step, where it grows slightly. For game (*b*), G2-O increases greatly starting in the sixth step. Later, G2-X also increases after the 9th step. However, G2-X ultimately stays at a very low level compared with G2-O. Thus, for both games, the circuit can determine the winner.

Experiment. For an experiment on the complete game, a total of 16 three-input AND gates and a cross-inhibitor have to be placed in one single tube in theory. To focus on explaining the role of the cross-inhibitor, the experimental process is simplified to reduce the leakage caused by the co-existence of many species. Note that for each player, the structures of the three-input AND gate are the same, regardless of whether it represents a horizontal line, a vertical line, or a diagonal line. For each game scenario, one AND gate corresponding to the line that is most likely to be formed is chosen for each player.

We test the game circuit by taking the two games shown in Figure 6C as examples. The order of the moves in game 1 is: x_1, o_5, x_2, o_3, x_4, o_7, x_6, o_9, x_8. Clearly, player O wins the game in the sixth step by forming a diagonal row. In game 2, the order of the moves is: x_1, o_5, x_2, o_4, x_7, o_6, x_8, o_3, x_9. Therefore, the winner of this game is still player O despite player X also forming a line in the end. In real games, it is unnecessary to make further moves after the winner has been determined. Note that although humans can directly recognize the winner of the game, such recognition is not an easy issue for DNA strand displacement circuits. The mechanism of cross-inhibition makes it possible to observe the final outcome when a game is finished rather than to detect whether a line has been formed at each step. Therefore, here we still consider this game scenario and take it as a test case for the cross-inhibitor.

In the experiment on game 1, the AND gate chosen for player X is X-456 (corresponding to complex T1 in Supplementary Table S1). For player O, O-357 (corresponding to complex T2 in Supplementary Table S1) is selected. In game 2, we use X-789 and O-456 (corresponding to T1 and T2 in Supplementary Table S1, respectively). For each of the experiments, the three-input AND gates and a cross-inhibitor (DA and DB in Supplementary Table S1) are initially added to the buffer in a tube. The concentration of each And gate is 400 nM and [DA] = [DB] = 200 nM. According to the rules of the game, no winner in any of the first four steps will be generated. Therefore, the DNA strands representing the first four moves are also added into the tube as substrates. Then, every 20 min, a DNA strand representing the next move is added. For example, in game 1, o3, o5 and o7 (represented by single strands IN2-1, IN2-2, and IN2-3 in Supplementary Table S2, respectively) that can trigger the gate O-357 to generate an output signal OB are added at steps 4, 2 and 6, respectively. x_4 and x_6 (represented by single strands IN1-1 and IN1-3 in Supplementary Table S2, respectively) that can react with gate X-456 are added at steps 5 and 7 respectively. The concentration ratio of each game piece to the And gate is 2.4.

The experimental results for these two games are shown in Figure 6D. In game 1, since no line is formed for player X, the concentration of OA (viz., G1-X) almost remains at a very low level until the ninth step. The concentra-

tion of OB (G1-O) increases at the time when a line is formed. It is direct to tell that the winner is player O. In game 2, since player O forms a line firstly, the concentration of OB (viz., G2-O) increases earlier and is finally higher than that of OA (viz., G2-X). G2-X has a considerable growth in the ninth step because SA is generated gradually by the three-input And gate rather than being added all at once.

When the game ends in a draw, the first module, viz., the three-input AND gate, will not be activated since no player produces a line. The result of such a game is straightforward since the concentrations of both OA and OB remain 0 the whole time. Therefore, there is no need to do the experiment for this case. Due to symmetry, the cases in which X wins the game are also omitted. Thus, it can be concluded that the cross-inhibitor mechanism is effective in creating a referee for a tic-tac-toe game, and this application shows the feasibility of the cross-inhibitor to the observation of some biochemical processes.

CONCLUSION

In this work, we developed a cross-inhibitor that can execute mutual inhibition, analyzed its performance in terms of time-response characteristics, controllability and expansibility, and demonstrated its effectiveness by performing a tic-tac-toe game as an example.

The cross-inhibitor implemented here can serve as a signal-controlling or signal-processing device in time-critical molecular systems, e.g. detecting the temporal order of two consecutive events. Being enzyme-free, this device is expected to be adaptable to other experimental environments, e.g. biochemical reaction cascade circuits with enzymatic digestion. Since this framework is modularly designed, more complex circuits could also be fabricated. Moreover, in the present circuit, one end of the detector has no toehold. By adding a toehold, the cascading function can be extended to be integrated into more complex biochemical reaction networks and to realize better control of DNA nanomachines.

The proposed device can be further explored in terms of its sensitivity. By optimizing the DNA sequences and enhancing the reaction environments, the reaction rate of producing OA (respectively, OB) in this circuit can be increased. Thus, more efficient signal inhibition of DB (DA) by DA (DB) can be realized.

The mechanism we designed is somewhat similar to the buffer gate of (54). Both mechanisms utilize toehold exchange to trigger the subsequent reaction and form a stable duplex in the end. However, dealing with transient signals via this kind of mechanism is relatively weak because the output signal will have a certain amount of attenuation when the input signal is removed because of the toehold produced by the toehold exchange. The Seelig-Soloveichik AND gate (25) provided inspiration for improvement. In this device, once the input signal occurs, a stable double-stranded product is generated through DNA strand displacement. In this way, the concentration of the output can remain unchanged if the input signal is removed. We will take advantage of this strategy as an expansion of our device.

As claimed in (45), 'Future nucleic acid control circuits must be interfaced to molecular sensors and actuators'. To establish larger and more complex biochemical reaction circuits, modular interfaces are essential because they can reduce the complexity of the underlying system and improve the efficiency and also ensure maintainability. In future work, we would like to extend the cross-inhibitor module by adding interfaces for upstream and downstream signals to connect it to molecular sensors or actuators. One possible way is to introduce a loop structure in the cross-inhibitor. The toehold hidden in the loop can be exposed to trigger downstream reactions when the reactions in the cross-inhibitor are completed. We can also extend the 5′end of domain a in DA and the 5′end of domain b in DB, and set the toehold domain appropriately so that the released strand can participate in the downstream reaction.

SUPPLEMENTARY DATA

Supplementary Data are available at NAR Online.

ACKNOWLEDGEMENTS

The authors would like to express their sincere gratitude to the anonymous reviewers for their constructive comments for improving our manuscript.

FUNDING

National Key R&D Program of China (No. 2018YFC0910500), the National Natural Science Foundation of China (Nos. 61425002, 61702075, 61772100, 61751203, 61872101), Young Elite Scientists Sponsorship Program by CAST (No. 2018QNRC001), Program for Changjiang Scholars and Innovative Research Team in University (No. IRT_15R07), the Program for Liaoning Innovative Research Team in University (No. LT2017012).
Conflict of interest statement. None declared.

REFERENCES

1. Chen,J. and Seeman,N.C. (1991) Synthesis from DNA of a molecule with the connectivity of a cube. *Nature*, **350**, 631–633.
2. Seeman,N.C. (1982) Nucleic acid junctions and lattices. *J. Theor. Biol.*, **99**, 237–247.
3. Groves,B., Chen,Y.J., Zurla,C., Pochekailov,S., Kirschman,J.L., Santangelo,P.J. and Seelig,G. (2016) Computing in mammalian cells with nucleic acid strand exchange. *Nat. Nanotechnol.*, **11**, 287–294.
4. Genot,A.J., Bath,J. and Turberfield,A.J. (2013) Combinatorial displacement of DNA strands: application to matrix multiplication and weighted sums. *Angew. Chem. Int. Ed.*, **52**, 1189–1192.
5. Tikhomirov,G., Petersen,P. and Qian,L. (2017) Fractal assembly of micrometre-scale DNA origami arrays with arbitrary patterns. *Nature*, **552**, 67.
6. Tikhomirov,G., Petersen,P. and Qian,L. (2016) Programmable disorder in random DNA tilings. *Nat. Nanotechnol.*, **12**, 251–259.
7. Evans,C.G. and Winfree,E. (2017) Physical principles for DNA tile self-assembly. *Chem. Soc. Rev.*, **46**, 3808–3829.
8. Abolhasan,R., Mehdizadeh,A., Rashidi,M.R., Aghebati-Maleki,L. and Yousefi,M. (2019) Application of hairpin DNA-based biosensors with various signal amplification strategies in clinical diagnosis. *Biosens. Bioelectron.*, **129**, 164–174.
9. Du,H., Yang,P., Hou,X., Zhou,R., Hou,X. and Chen,J. (2019) Expanding DNA nanomachine functionality through binding-induced DNA output for application in clinical diagnosis. *Chem. Commun.*, **55**, 3610–3613.

10. Dou,B., Yang,J., Shi,K., Yuan,R. and Xiang,Y. (2016) DNA-mediated strand displacement facilitates sensitive electronic detection of antibodies in human serums. *Biosens. Bioelectron.*, **83**, 156–161.
11. Liu,N., Xu,K., Liu,L., Chen,X., Zou,Y. and Xiao,X. (2018) A star-shaped DNA probe based on strand displacement for universal and multiplexed fluorometric detection of genetic variations. *Microchim. Acta*, **185**, 413.
12. Wang,J.S. and Zhang,D.Y. (2015) Simulation-guided DNA probe design for consistently ultraspecific hybridization. *Nat. Chem.*, **7**, 545–553.
13. Fern,J., Scalise,D., Cangialosi,A., Howie,D., Potters,L. and Schulman,R. (2017) DNA strand displacement timer circuits. *ACS Synth. Biol.*, **6**, 190–193.
14. Li,W., Zhang,F., Yan,H. and Liu,Y. (2016) DNA based arithmetic function: a half adder based on DNA strand displacement. *Nanoscale*, **8**, 3775–3784.
15. Qian,L. and Winfree,E. (2011) Scaling up digital circuit computation with DNA strand displacement cascades. *Science*, **332**, 1196–1201.
16. Song,T.S., Garg,S., Mokhtar,R., Bui,H. and Reif,J. (2016) Analog computation by DNA strand displacement circuits. *ACS Synth. Biol.*, **5**, 898–921.
17. Li,W., Yang,Y., Yan,H. and Liu,Y. (2013) Three-input majority logic gate and multiple input logic circuit based on DNA strand displacement. *Nano Lett.*, **13**, 2980–2988.
18. Chatterjee,G., Dalchau,N., Muscat,R.A., Phillips,A. and Seelig,G. (2017) A spatially localized architecture for fast and modular DNA computing. *Nat. Nanotechnol.*, **12**, 920.
19. Kroener,F., Heerwig,A., Kaiser,W., Mertig,M. and Rant,U. (2017) Electrical actuation of a DNA origami nanolever on an electrode. *J. Am. Chem. Soc.*, **139**, 16510–16513.
20. Ranallo,S., Prévost-Tremblay,C., Idili,A., Vallée-Bélisle,A. and Ricci,F. (2017) Antibody-powered nucleic acid release using a DNA-based nanomachine. *Nat. Commun.*, **8**, 15150.
21. Li,P., Xie,G., Liu,P., Kong,X., Song,Y., Wen,L. and Jiang,L. (2018) Light-driven ATP transmembrane transport controlled by DNA nanomachines[J]. *J. Am. Chem. Soc.*, **140**, 16048–16052.
22. Zhang,P., Jiang,J., Yuan,R., Zhuo,Y. and Chai,Y. (2018) Highly ordered and field-free 3D DNA nanostructure: the next generation of DNA nanomachine for rapid single-step sensing. *J. Am. Chem. Soc.*, **140**, 9361–9364.
23. Seeman,N.C. (2007) An overview of structural DNA nanotechnology. *Mol. Biotechnol.*, **37**, 246–257.
24. Zhang,D.Y. and Seelig,G. (2011) Dynamic DNA nanotechnology using strand displacement reactions. *Nat. Chem.*, **3**, 103–113.
25. Seelig,G., Soloveichik,D., Zhang,D.Y. and Winfree,E. (2006) Enzyme-free nucleic acid logic circuits. *Science*, **314**, 1585–1588.
26. Srinivas,N., Ouldridge,T.E., Sulc,P., Schaeffer,J.M., Yurke,B., Louis,A.A., Doye,J.P. and Winfree,E. (2013) On the biophysics and kinetics of toehold mediated DNA strand displacement. *Nucleic Acids Res.*, **41**, 10641–10658.
27. Xing,Y., Yang,Z. and Liu,D. (2011) A responsive hidden toehold to enable controllable DNA strand displacement reactions. *Angew. Chem. Int. Ed.*, **50**, 11934–11936.
28. Xu,Y., Zhou,W., Zhou,M., Xiang,Y., Yuan,R. and Chai,Y. (2015) Toehold strand displacement-driven assembly of G-quadruplex DNA for enzyme-free and non-label sensitive fluorescent detection of thrombin. *Biosens. Bioelectron.*, **64**, 306–310.
29. Lakin,M.R. and Stefanovic,D. (2016) Supervised learning in adaptive DNA strand displacement networks. *ACS Synth. Biol.*, **5**, 885–897.
30. Chiniforooshan,E., Doty,D., Kari,L. and Seki,S. (2010) Scalable, time-responsive, digital, energy-efficient molecular circuits using DNA strand displacement. In: *Proceedings of the 16th International Conference on DNA Computing and Molecular Programming (DNA'10)*. Springer-Verlag, Berlin, Heidelberg, pp. 25–26.
31. Thubagere,A.J., Thachuk,C., Berleant,J., Johnson,R.F., Ardelean,D.A., Cherry,K.M. and Qian,L.L. (2017) Compiler-aided systematic construction of large-scale DNA strand displacement circuits using unpurified components. *Nat. Commun.*, **8**, 14373.
32. Zhang,Z., Fan,T.W. and Hsing,I.-M. (2017) Integrating DNA strand displacement circuitry to the nonlinear hybridization chain reaction. *Nanoscale*, **9**, 2748–2754.
33. Yao,D., Song,T., Sun,X., Xiao,S., Huang,F. and Liang,H. (2015) Integrating DNA Strand-Displacement Circuitry with Self-Assembly of Spherical Nucleic Acids. *J. Am. Chem. Soc.*, **137**, 14107–14113.
34. Zhang,D.Y., Hariadi,R.F., Choi,H.M.T. and Winfree,E. (2013) Integrating DNA strand-displacement circuitry with DNA tile self-assembly. *Nat. Commun.*, **4**, 1965.
35. Kay,E.R., Leigh,D.A. and Zerbetto,F. (2007) Synthetic molecular motors and mechanical machines. *Angew. Chem. Int. Ed.*, **46**, 72–191.
36. Bath,J. and Turberfield,A.J. (2007) DNA nanomachines. *Nat. Nanotech.*, **2**, 275–284.
37. Li,L., Li,N., Fu,S., Deng,Y., Yu,C. and Su,X. (2019) Base excision repair-inspired DNA motor powered by intracellular apurinic/apyrimidinic endonuclease. *Nanoscale*, **11**, 1343–1350.
38. Thubagere,A.J., Li,W., Johnson,R.F., Chen,Z., Doroudi,S., Lee,Y.L., Izatt,G., Wittman,S., Srinivas,N., Woods,D. *et al.* (2017) A cargo-sorting DNA robot. *Science*, **357**, eaan6558.
39. Qian,L. and Winfree,E. (2011) A simple DNA gate motif for synthesizing large-scale circuits. *J. R. Soc. Interface*, **8**, 1281–1297.
40. Qian,L., Winfree,E. and Bruck,K. (2011) Neural network computation with DNA strand displacement cascades. *Nature*, **475**, 368–372.
41. Zhou,C., Duan,X. and Liu,N. (2015) A plasmonic nanorod that walks on DNA origami. *Nat. Commun.*, **6**, 8102.
42. Hong,F., Zhang,F. and Liu,Y. (2017) DNA origami: scaffolds for creating higher order structures. *Chem. Rev.*, **117**, 12584–12640.
43. Erbas-Cakmak,S., Leigh,D.A. and Mcternan,C.T. (2015) Artificial molecular machines. *Chem. Rev.*, **115**, 10081–10206.
44. Zhang,D.Y. and Winfree,E. (2009) Control of DNA strand displacement kinetics using toehold exchange. *J. Am. Chem. Soc.*, **131**, 17303–17314.
45. Zhang,D.Y., Turberfield,A.J., Yurke,B. and Winfree,E. (2007) Engineering entropy-driven reactions and networks catalyzed by DNA. *Science*, **318**, 1121–1125.
46. Du,Y., Han,X., Wang,C., Li,Y., Li,B. and Duan,H. (2017) Smart sensing based on DNA-Metal interaction enables a Label-Free and resettable security model of electrochemical molecular keypad lock. *ACS sensors*, **3**, 54–58.
47. Groves,B., Chen,Y.J., Zurla,C., Pochekailov,S., Kirschman,J.L., Santangelo,P.J. and Seelig,G. (2016) Computing in mammalian cells with nucleic acid strand exchange. *Nat. Nanotechnol.*, **11**, 287–294.
48. Stojanovic,M.N. and Stefanovic,D. (2003) A deoxyribozyme-based molecular automaton. *Nat. Biotechnol.*, **21**, 1069–1074.
49. Li,C., Li,Y., Chen,Y., Lin,R., Li,T., Liua,F. and Li,N. (2016) Modulating the DNA strand-displacement kinetics with the one-sided remote toehold design for differentiation of single-base mismatched DNA. *RSC Advances*, **6**, 74913–74916.
50. Fogel,D. B. (1993) Using evolutionary programing to create neural networks that are capable of playing tic-tac-toe. *IEEE International Conference on Neural Networks*, **2**, 875–880.
51. Grim,J., Somol,P. and Pudil,P. (2005) Probabilistic neural network playing and learning Tic-Tac-Toe. *Pattern Recognition Letters*, **26**, 1866–1873.
52. Cherry,K.M. and Qian,L. (2018) Scaling up molecular pattern recognition with DNA-based winner-take-all neural networks. *Nature*, **559**, 370–376.
53. Chen,Y.J., Dalchau,N., Srinivas,N., Phillips,A., Cardelli,L., Soloveichik,D. and Seelig,G. (2013) Programmable chemical controllers made from DNA. *Nat. Nanotechnol.*, **8**, 755.
54. Cardelli,L. (2011) Strand algebras for DNA computing. *Nat. Comput.*, **10**, 407–428.